EXHIBIT G

ELSEVIER

Biomaterials 23 (2002) 699–710

Biomaterials

www.elsevier.com/locate/biomaterials

Mechanochemical–hydrothermal synthesis of carbonated apatite powders at room temperature

Wojciech L. Suchanek[a], Pavel Shuk[a,1], Kullaiah Byrappa[a,2], Richard E. Riman[a,*], Kevor S. TenHuisen[b], Victor F. Janas[b]

[a] *Department of Ceramic and Materials Engineering, Rutgers, The State University of New Jersey, 607 Taylor Road, Piscataway, NJ 08854-8087, USA*

[b] *Johnson & Johnson Corporate Biomaterials Center, Rt. 22 W, P.O. Box 151, Somerville, NJ 08876-0151, USA*

Received 20 November 2000; accepted 16 April 2001

Abstract

Crystalline carbonate- and sodium-and-carbonate-substituted hydroxyapatite (CO_3HAp and $NaCO_3$HAp) powders were prepared at room temperature via a heterogeneous reaction between $Ca(OH)_2/CaCO_3/Na_2CO_3$ and $(NH_4)_2HPO_4$ aqueous solution using the mechanochemical–hydrothermal route. X-ray diffraction, infrared spectroscopy, thermogravimetry, and chemical analysis were performed. Room temperature products were phase-pure CO_3HAp and $NaCO_3$HAp containing 0.8–12 wt% of carbonate ions in the lattice. Dynamic light scattering revealed that the median agglomerate size of the room temperature CO_3HAp and $NaCO_3$HAp powders was in the range of 0.35–1.6 μm with a specific surface area between 82 and 121 m^2/g. Scanning and transmission electron microscopy confirmed that the carbonated HAp powders consisted of mostly submicron aggregates of nanosized, ≈20 nm crystals. The synthesized carbonated apatite powders exhibit chemical compositions and crystallinities similar to those of mineral constituents of hard tissues and therefore are promising for fabrication of bone-resembling implants.

Keywords: Carbonate apatite; Hydroxyapatite; Biocompatibility; Mechanochemical synthesis; Hydrothermal synthesis; Powder

1. Introduction

Hydroxyapatite (HAp) with the chemical formula corresponding to $Ca_{10}(PO_4)_6(OH)_2$, has been extensively used in medicine for implant fabrication and is one of the most biocompatible materials owing to its similarity with mineral constituents found in hard tissue (i.e. teeth and bones) [1,2]. It is commonly the material of choice for fabrication of dense and porous HAp bioceramics [3]. Its general uses include biocompatible phase/reinforcement in composites [4], coatings on metal implants [1–3], and granular fill for direct incorporation into human tissues [1]. Among the variety of HAp-based ceramics, carbonated HAp (CO_3HAp) appears to be an excellent material for bioresorbable bone substitutes [5]. Since the HAp phase present in natural bone, dentin, and enamel, respectively, contains approximately 7.4, 5.6, and 3.5 wt% of carbonate [6], CO_3HAp materials have excellent biocompatibility and properties, which can be favorably compared with those of hard tissue.

Sintered CO_3HAp ceramics can exhibit in vitro cell resorption rates similar to the resorption rate of natural bone minerals [5], which is higher than that of pure HAp ceramics [5,7]. Cell appearance and proliferation does not differ on CO_3HAp and pure HAp [7,8]. Recent in vivo study using rats indicated that the dissolution rate of dense sintered CO_3HAp ceramics implanted subcutaneously was intermediate between β-TCP and pure HAp [9]. In another in vivo study, it was found that the quantity of intermedullar bone formed around CO_3HAp implants increased with carbonate concentration [10]. CO_3HAp-forming injectable, moldable bone cement has been commercially available throughout Europe since 1997 and in the USA since 1998 [11]. The CO_3HAp bone cements can be used as in situ-hardened bone fillers [12] or screw fixations [13]. Nanosized CO_3HAp crystals were successfully applied to fabricate

*Corresponding author. Tel.: +1-732-445-4946; fax: +1-732-445-6264.

E-mail address: riman@alumina.rutgers.edu (R.E. Riman).

[1] Present address: Rosemount Analytical Inc., 1201 North Main Street, P.O. Box 901, Orrville, Ohio 4467-0901, USA.

[2] Permanent address: Department of Geology, University of Mysore, P.B. No. 21, Mysore-570 006, India.

0142-9612/02/$ - see front matter
PII: S0142-9612(01)00158-2

CO_3HAp/collagen biodegradable composites [14]. When implanted in rabbits, these materials underwent resorption and promoted new bone formation.

The above studies indicate that CO_3HAp ceramics should be superior to pure HAp for bioresorbable implants. Therefore, development of new synthesis techniques for CO_3HAp powders with controlled morphology and chemical composition is of a great importance. CO_3HAp powders with low crystallinity and nanometer particle size are suitable for the processing of bone-resembling materials [14]. In addition, controlling the level of carbonate substitution in HAp is a convenient way to change solubility [6] and morphology of the synthesized carbonated HAp crystals [6], which subsequently impact properties of the HAp-based biomaterials.

Multiple techniques have been used to prepare HAp and CO_3HAp powders, with wet chemical methods [1,3,6,15,16] and solid-state reactions [1,17] as the most popular. Depending upon the technique, powders with different morphologies, stoichiometries and levels of crystallinity can be obtained. Recently, several papers regarding mechanochemical and mechanochemical–hydrothermal synthesis of HAp and CO_3HAp powders appeared in the literature [18–25]. Mechanochemical powder synthesis is a solid-state synthesis method that takes advantage of the perturbation of surface-bonded species by pressure to enhance thermodynamic and kinetic reactions between solids [26]. In many cases, mechanochemistry can be used to prepare anhydrous multi-component oxides at room temperature in a single step. Pressure can be applied via conventional milling equipment ranging from low-energy ball mills to high-energy stirred mills (e.g. attrition, planetary, or vibratory mills). The main advantages of mechanochemical synthesis of ceramic powders are simplicity and low cost. A variety of chemical compounds have been prepared by this technique, such as $CaSiO_3$ [27], $PbTiO_3$ [28], and $0.9Pb(Mg_{1/3}Nb_{2/3})O_3$-$0.1PbTiO_3$ [29]. Since the mechanochemical synthesis involves only solid-state reaction, it should be clearly distinguished from the mechanochemical–hydrothermal synthesis (a.k.a., "wet" mechanochemical), which incorporates an aqueous phase in the system. An aqueous phase can actively participate in the mechanochemical reaction by accelerating kinetic processes that commonly rate limit a process, such as dissolution, diffusion, adsorption, reaction rate, and crystallization (nucleation and growth) [30]. The mechanochemical activation of slurries can generate local zones of high temperatures (up to 450–700°C) and high pressures due to friction effects and adiabatic heating of gas bubbles (if present in the slurry), while the overall temperature is close to the room temperature [31]. Thus, the mechanochemical–hydrothermal technique can be envisioned as being located at the intersection of hydrothermal [32] and mechanochemical [26] processing. The mechanochemical–hydrothermal route can produce large amounts of HAp powder. It also utlizes lower temperature, i.e. room temperature, as compared to 90–200°C for the hydrothermal process. Thus, for the mechanochemical–hydrothermal process, there is no need for a pressure vessel and external heating.

In an earlier study we have demonstrated that stoichiometric, crystalline HAp powder could be prepared at room temperature from heterogeneous reaction between $Ca(OH)_2$ powder and $(NH_4)_2HPO_4$ solution via the mechanochemical–hydrothermal route [25]. This process was advantageous when compared to prior reported mechanochemical HAp syntheses. Water actively participated in the reaction by both dissolving one of the reactant powders, as well as serving as a reaction medium to produce a stoichiometric and highly crystalline product. In addition, the mechanochemical–hydrothermal route has been demonstrated to be applicable for reproducible and low-cost fabrication of high-quality HAp powders in large batch sizes [25]. In this paper, we will present a mechanochemical–hydrothermal method for preparation of nanocrystalline CO_3HAp and $NaCO_3$HAp powders with controlled carbonate substitution.

2. Materials and methods

2.1. Mechanochemical–hydrothermal preparation of carbonated HAp powders

Calcium hydroxide powder ($Ca(OH)_2$), calcium carbonate powder ($CaCO_3$), and solid diammonium hydrogen phosphate ($(NH_4)_2HPO_4$) (all analytical grade, Alfa Aesar, Ward Hill, MA) were used as reactants for synthesis of CO_3-substituted HAp. For synthesis of HAp powders with coupled CO_3- and Na-substitution, sodium carbonate (Na_2CO_3) (analytical grade, Alfa Aesar, Ward Hill, MA) was used instead of $CaCO_3$. Purity of the reactants was confirmed by X-ray diffraction and thermogravimetry. Measured contents of adsorbed water in $Ca(OH)_2$, $(NH_4)_2HPO_4$, $CaCO_3$, and Na_2CO_3 were 1.9, 1.1, 0.8, and 1.0 wt.%, respectively. All stoichiometries were appropriately adjusted to compensate for the adsorbed water. No impurity phases were present in the starting powders. Targeted chemical compositions corresponded to x values of 0, 1, 2, and 3 in the chemical formula of $Ca_{10-x+y}(CO_3)_x(PO_4)_{6-x}(OH)_{2-x+2y}$ for CO_3-substituted HAp (denoted hereafter CO_3HAp) and $x=0$, 1, 2, 3, 4 in the chemical formula of $Ca_{10-x}Na_{2x/3}(PO_4)_{6-x}(CO_3)_x(H_2O)_x(OH)_{2-x/3}$ for Na- and CO_3-substituted HAp (denoted hereafter $NaCO_3$HAp).

Both CO_3HAp and $NaCO_3$HAp powders were synthesized according to the following procedure. First,

a suspension of $Ca(OH)_2$ and $CaCO_3$ (or Na_2CO_3), a total of about 26–32 g as required by stoichiometry, in 350 ml of deionized water was prepared inside a 500 ml glass beaker. Subsequently, stoichiometric amounts of $(NH_4)_2HPO_4$ powder (20–27 g) was slowly added to the same beaker at constant vigorous stirring using a magnetic stirrer for about 10 min. The concentration of the solid phase in each slurry was 13 wt%, which yielded a measured pH of 10.0–11.3. Slurry pH was measured using a glass electrode connected to a pH-meter (Accumet® Model 805 MP, Fisher Scientific, Pittsburgh, PA) and calibrated with respect to a buffer solution (pH = 10.00, Fisher Scientific, Pittsburgh, PA). The mechanochemical–hydrothermal synthesis was performed by placing slurries into a laboratory-scale mill (model MIC-0, NARA Machinery Co., Tokyo, Japan) equipped with a zirconia liner and zirconia ring grinding media.

The milling equipment is a multi-ring media mill and its grinding mechanism is different from other attrition, planetary, or vibratory mills (Fig. 1) [33]. The mill consists of a central rotating stainless-steel shaft, which drives six stainless-steel sub-shafts (sleeve-lined with zirconia-toughened alumina) that are connected symmetrically to the central shaft. Each sub-shaft contains 19 stacked zirconia rings, which can rotate eccentrically around each sub-shaft. When the central shaft is rotating, the zirconia rings on the sub-shafts are moved by the centrifugal force radially outwards applying force on a ceramic liner which is mounted on an inner wall of the milling vessel. Solid particles, which are located between the rotating rings and the liner wall, are subsequently comminuted [33].

Grinding of the slurry was carried out in air, initially at a rotation speed of 1500 rpm for 1 h and then at 800 rpm for 4 h. Temperature during the grinding was measured using a thermocouple, which ranged between 29–35°C at 1500 rpm and 25–32°C at 800 rpm depending upon the batch. After the mechanochemical–hydrothermal reaction, the suspension was centrifuged and decanted. The resultant powder was washed with distilled water in HDPE 250 ml bottles using a hand shaker machine (Model M37615, Barnstead/Thermolyne, Dubuque, Iowa) followed by centrifuging at 4500 rpm for 30 min (Induction Drive Centrifuge, Model J2-21M, Beckman Instruments, Fullerton, CA). Each batch of powder was washed 6 times. The washed HAp powders were dried in an oven at 70°C for 24 h (Isotemp® oven, model 230G, Fisher Scientific, Pittsburgh, PA). These powders are referred to as "as-prepared" in the paper. A typical mass of as-prepared dry carbonated HAp powder was about 30 g per batch.

In order to check thermal stability of the prepared CO_3HAp and $NaCO_3HAp$ phases herein referred to as "heat-treated", a small quantity of each as-prepared powder was placed in an alumina crucible, ramped to

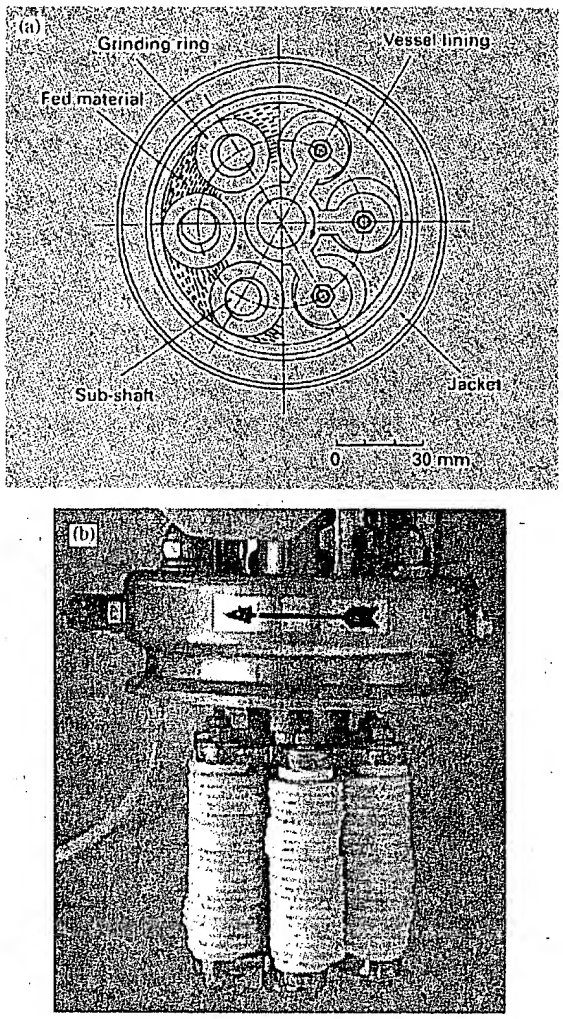

Fig. 1. Multi-ring media mill MiCROS MIC-O (NARA Machinery Co.): (a) cross-section of the mill showing schematic of the grinding mechanism; (b) interior of the mill showing sub-shafts with ZrO_2 milling rings surrounding the central shaft.

temperature at a rate of 10°C/min and heat treated in air at 1100°C for 1 h (Rapid Temperature Furnace, CM Inc., Bloomfield, NJ). The samples were cooled together with the furnace to room temperature (average cooling rate ≈6°C/min) and removed. All heat-treated CO_3HAp and $NaCO_3HAp$ powders were stored in air atmosphere without humidity/carbon dioxide control.

2.2. Characterization of the materials

All batches of as-prepared and heat-treated CO_3HAp and $NaCO_3HAp$ powders were characterized by X-ray diffraction (XRD, Kristalloflex D-500, Siemens Analytical X-ray Instrument Inc., Madison, WI) using Ni filtered Cu K_α radiation, in the 2θ range of 10–70° at a

scan rate of 2.4°/min, with a sampling interval of 0.05°. Crystallographic identification of the as-prepared and heat-treated HAp powders was accomplished by comparing the experimental XRD patterns to standards compiled by the Joint Committee on Powder Diffraction and Standards (JCPDS), which were card #9-432 for HAp, #9-169 for β-TCP, #37-1497 for CaO, #05-0586 for $CaCO_3$, #04-0733 for $Ca(OH)_2$, and #75-0642 for NaOH.

Specific surface area of all batches of as-prepared CO_3HAp and $NaCO_3$HAp powders was measured using the BET method utilizing adsorption of N_2 gas (purity 99.99%, Matheson Co., Bridgeport, NJ) at −196°C (Coulter Surface Area Analyzer SA 3100, Coulter Co., Fullerton, CA). For this purpose, 0.15–0.30 g of the HAp powder was outgased for 2–4 h at 120°C. Particle size of the primary crystals was estimated from the nitrogen adsorption isotherms using the BET method to calculate the equivalent spherical diameter, also called a BET particle diameter (d_{BET}), from the following equation: $d_{BET}=6/(\rho S_w)$, where ρ is density and S_w is the specific surface area. A density of 3.156 g/cm^3 which is the theoretical density of stoichiometric HAp, was used in all calculations.

Particle size distributions of all batches of as-prepared CO_3HAp and $NaCO_3$HAp powders were determined by dynamic light scattering at a wavelength of 632.8 nm (DLS, model DLS-700, Otsuka Electronics Co., Osaka, Japan). Samples for the DLS measurements were prepared by dispersing small amounts of the HAp powder in ethanol (filtered using a 0.2 μm filter) followed by immersion in an ultrasonic bath for 10 min. After transferring to the sample holder, the suspensions were diluted again using filtered ethanol and ultrasonicated for 3 min. Measurement conditions with a sampling time of 100 μs and 100 accumulations were employed. A viscosity of 1.19 cP and refractive index of 1.36 were used for calculations.

Size and degree of aggregation of the synthesized particles in selected batches of as-prepared HAp and $NaCO_3$HAp were studied using a field emission scanning electron microscope at 0.5–1.1 kV with a working distance of 2–3 mm (FESEM, Model DSM 962, Gemini, Carl Zeiss Inc., Thornwood, NY). Prior to the FESEM analysis, the as-prepared samples were suspended in ethanol and dispersed for 10 min using ultrasound. Subsequently, they were transferred on graphite sheets mounted onto sample holders. No conductive coatings were used.

Transmission electron microscopy study of the as-prepared powders was performed using an ultra-high resolution analytical electron microscope (TEM, model EM-002B, International Scientific Instruments, Pleasanton, CA) at an accelerating voltage of 200 kV. In order to prepare samples for the TEM, small quantities of the as-prepared powders were dispersed in ethanol, ultrasonicated for 5 min, transferred onto carbon grids, and subsequently dried at 40°C for 24 h.

Infrared spectra of all batches of as-prepared CO_3HAp and $NaCO_3$HAp powders were obtained using an infrared, Fourier-transform spectrometer (FTIR, model 1720-X, Perkin Elmer Co., Norwalk, CT). For this purpose, each powder was mixed with KBr in the proportion 1/150 (by weight) for 15 min and pressed into a pellet using a hand press.

Thermogravimetric analysis (model TGA-6, Perkin Elmer Co., Norwalk, CT) for all batches of as-prepared CO_3HAp and $NaCO_3$HAp powders was performed in air at a flow rate of 20 ml/min. Samples were heated to a maximum temperature of 950°C using a heating rate of 5°/min.

Quantitative analysis for sodium and carbonate was accomplished for all batches of as-prepared CO_3HAp and $NaCO_3$HAp powders at the Materials Characterization Laboratory of the Pennsylvania State University (University Park, PA). The analysis for sodium was accomplished by DC plasma emission spectrometry after dissolution of the powdered samples in HCl (aq). The analysis for CO_2 was accomplished by carbon dioxide coulometry [34]. Maximum relative error of the chemical analysis by these techniques was 5% of the measured value.

3. Results and discussion

3.1. CO_3-substituted HAp powders

XRD patterns of the as-prepared CO_3HAp powders are shown in Fig. 2. The XRD peaks are well defined and attributable only to apatite lattice planes for $x=0$ (i.e. nominal stoichiometric HAp) (Fig. 2a), $x=1$ (Fig. 2b), and $x=2$ (Fig. 2c). When a large excess of $CaCO_3$, corresponding to the x value of 3, was used in the starting slurry, unreacted $CaCO_3$ in the synthesis product was found (Fig. 2d). The sample containing apatite with the unreacted calcite ($x=3$) was excluded from any further evaluation.

Results of the thermogravimetric analysis of the as-prepared CO_3HAp powders in the temperature range of 25–950°C are shown in Fig. 3. Significant loss of weight was observed up to approximately 450°C for all samples and was due to the loss of adsorbed (up to ≈120°C) and lattice water [15]. Another significant and gradual weight loss of CO_3HAp powders occurred above 550°C, which is attributed mostly to the loss of carbonate with subsequent formation of CaO (Fig. 3b and c). In contrast, the HAp powder with nominal stoichiometric composition (Fig. 3a) exhibited no significant weight loss above 500°C, typical for stoichiometric HAp [15]. In apatites, lattice water can also be lost in this temperature region [15], but the total amount

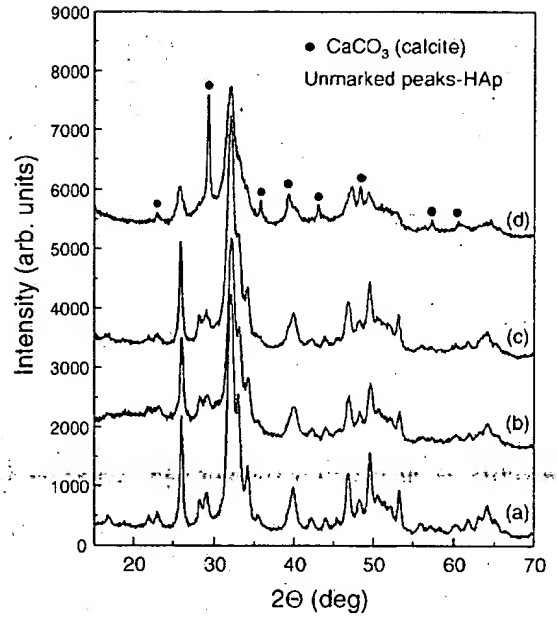

Fig. 2. XRD patterns of the as-prepared CO_3HAp powders: (a) $x=0$, corresponding to stoichiometric HAp; (b) $x=1$; (c) $x=2$; and (d) $x=3$.

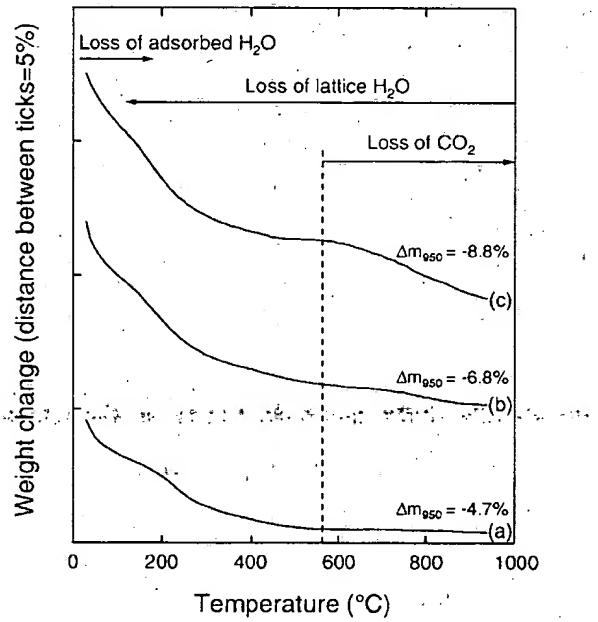

Fig. 3. TG curves of the as-prepared CO_3HAp powders: (a) $x=0$; (b) $x=1$; and (c) $x=2$. Δm_{950} is a total relative weight change at 950°C. The Δm_{950} values are marked for each powder.

of lattice water accounts for no more than about 2% of the total weight in apatite. Weight losses related to the decomposition of unreacted $CaCO_3$ or $Ca(OH)_2$ were not observed, which in addition to the XRD data serves as evidence that the synthesized powder was phase pure CO_3HAp. $Ca(OH)_2$ or $CaCO_3$, if present as an impurity

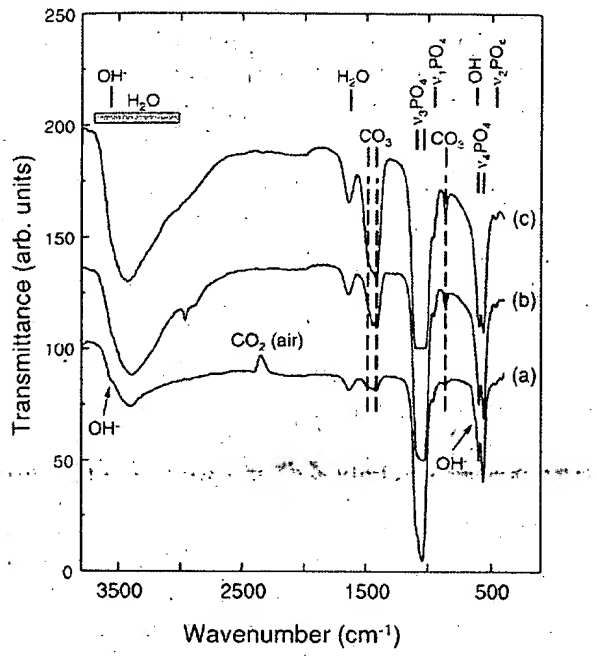

Fig. 4. FTIR spectra of the as-prepared CO_3HAp powders: (a) $x=0$; (b) $x=1$; and (c) $x=2$.

phase in the as-prepared HAp powders, would produce distinct rapid weight losses at 400–450°C (decomposition temperature of $Ca(OH)_2$) and 825°C (decomposition temperature of $CaCO_3$), as opposed to a continuous gradual weight loss, which was observed in our substituted HAp powders at those temperatures. However, small quantities of amorphous calcium phosphate, undetectable by XRD, TG and FTIR, might be present in the samples.

FTIR spectra of the as-prepared CO_3HAp powders are shown in Fig. 4. These are typical spectra of carbonated HAp showing PO_4-derived bands at 478, 566, 605, 963, and 1030–1090 cm^{-1}, and CO_3-derived bands at 870 cm^{-1} and around 1420–1480 cm^{-1} [6,15]. Adsorbed water bands are located at 1630 and 3000–3700 cm^{-1}. Low intensity of both OH-derived bands at 630 and 3570 cm^{-1}, which are clearly visible only in the nominally stoichiometric HAp powder (Fig. 4a), and broadening of the PO_4-derived bands with increasing x were observed. These effects are typical for CO_3HAp synthesized by wet methods and can be explained by a decrease of crystallinity due to increased carbonate substitution in the HAp lattice [6]. Since the intensity of the adsorbed water bands increased with increasing x, very low intensity of the OH-derived bands, particularly in the samples with $x>0$, could also be caused by the presence of adsorbed water (Fig. 4, Table 1). The FTIR spectra clearly show that with increasing x in the starting slurry, intensity of the CO_3-derived bands increases which serves as evidence that the amount of carbonate in the HAp lattice increases.

Table 1
Properties of the as-prepared CO_3HAp and $NaCO_3HAp$ powders

Targeted chemical composition of the Powder	Measured concentration of CO_3^{2-} (wt%)	Specific surface area (m^2/g)	Equivalent spherical diameter, d_{BET} (nm)	Average particle size (nm)	Median particle size (nm)
HAp ($x=0$)	0.80	91.0	21.0	685	663
CO_3HAp ($x=1$)	2.45	83.5	22.8	818	900
CO_3HAp ($x=2$)	4.35	85.9	22.1	510	394
$NaCO_3HAp$ ($x=1$)	4.10	117	16.2	473	349
$NaCO_3HAp$ ($x=2$)	4.45	81.7	23.3	1285	1625
$NaCO_3HAp$ ($x=3$)	9.05	121.1	15.7	1298	1592
$NaCO_3HAp$ ($x=4$)	12.00	85.8	22.2	669	622

Measured concentrations of CO_3 in our CO_3HAp powders were 0.8 wt% for $x=0$, 2.45 wt% for $x=1$ and 4.35 wt% for $x=2$. The widely accepted chemical formula of CO_3HAp is $Ca_{10-x+y}(CO_3)_x(PO_4)_{6-x}(OH)_{2-x+2y}$, where $0 \leqslant x \leqslant 2$, and $2y \leqslant x$, corresponding to the theoretical solubility limit of carbonate in HAp of 14.6 wt% [35]. The solubility limit does not seem to be exceeded in any of the as-prepared CO_3HAp powders. The position of the carbonate-derived bands indicates that CO_3^{2-}-for-PO_4^{3-} substitution dominates in the CO_3HAp powders but some fraction of the OH^- groups might be replaced by the CO_3^{2-} groups, which is usually observed in carbonated HAp powders prepared by wet methods [6,15]. Increasing concentration of carbonate with x in the CO_3HAp powders, which increases lattice disorder, can partially explain broadening of the XRD peaks with increasing x (Fig. 2).

Heat treatment of the as-prepared CO_3HAp powders at 1100°C for 1 h in air resulted in narrowing their HAp-derived XRD peaks, which was caused by increasing crystal size (Fig. 5). The low intensity of the strongest peak attributed to β-TCP [(0120), $2\Theta \approx 31°$] in the heat-treated HAp powder with nominal stoichiometric composition ($x=0$) (Fig. 5a) serves as evidence that the HAp prepared by the mechanochemical–hydrothermal route is almost stoichiometric with some minor calcium deficiency ($Ca/P \leqslant 1.67$). The presence of $CaCO_3$ and CaO was observed in the heat-treated CO_3HAp powders, where $x=1$ and 2 (Fig. 5b and c). Since the as-prepared CO_3HAp powders did not contain any impurity-phases, as indicated by XRD, TG, and FTIR, the only possibility is that formation of CaO and $CaCO_3$ was a result of decomposition of CO_3HAp at high temperature. Formation of CaO in heat-treated CO_3HAp powders is often observed since the carbonate replacement of the phosphate groups increases the Ca/P molar ratio to values higher that 1.67 [15]. The $CaCO_3$ phase originated from the initially formed CaO during poorly controlled storage of the heat-treated samples in air atmosphere. CaO has been known to transform into $Ca(OH)_2$ and/or $CaCO_3$ upon storage in air [36,37].

Specific surface area of the as-prepared CO_3HAp powders ranged between 83 and 91 m^2/g ($\pm 2\,m^2/g$),

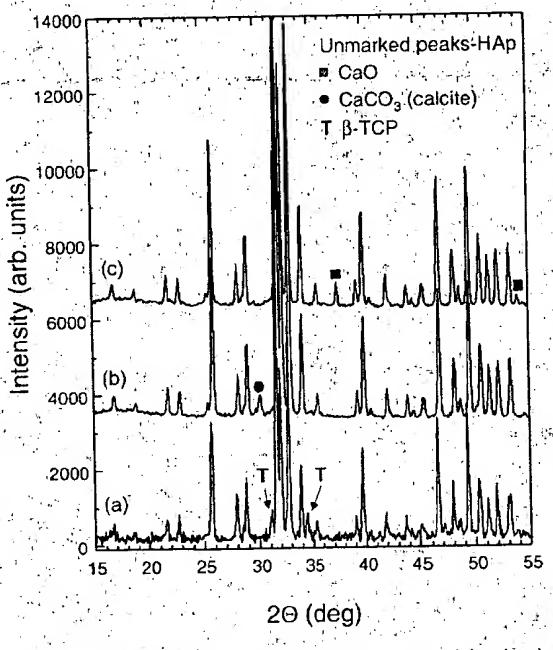

Fig. 5. XRD patterns of the CO_3HAp powders after calcination in air at 1100°C for 1 h: (a) $x=0$; (b) $x=1$; and (c) $x=2$.

which corresponds to an estimated equivalent spherical diameter (d_{BET}) of 21–23 nm (Table 1). Thus, in addition to lattice disorder introduced by the carbonate ions, the very small crystallite size also contributed to broadening of the XRD peaks (Fig. 2). The particle size distributions of the as-prepared CO_3HAp powders were monomodal in all cases with median values of 663 nm for $x=0$, 900 nm for $x=1$ and 394 nm for $x=2$ (Table 1). Corresponding average particle sizes were 685 nm for $x=0$, 818 nm for $x=1$ and 510 nm for $x=2$ (Table 1). The particle size distribution combined with the surface area data indicates the presence of aggregates consisting of ≈ 20 nm primary particles. Results of TEM observations, shown in Fig. 6, were in agreement with the results of both the BET and DLS measurements. The as-prepared CO_3HAp powders consisted of elongated aggregates of nanosized crystals (Fig. 6). The crystal size of both CO_3HAp powders was almost the same,

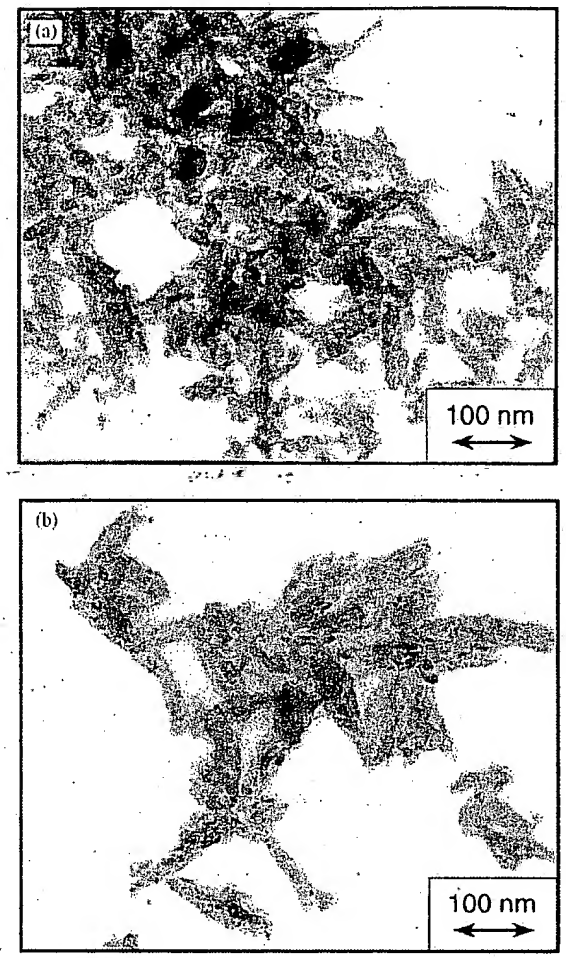

Fig. 6. TEM photographs of the as-prepared CO_3HAp powders showing aggregation of nanosized HAp crystals: (a) $x=1$, (b) $x=2$.

corresponding to similar values of the specific surface area and d_{BET} size.

3.2. Coupled Na- and CO_3-substituted HAp powders

XRD patterns of the as-prepared $NaCO_3$HAp powders are shown in Fig. 7. The XRD peaks are well defined and attributable only to apatite lattice planes for all x values ranging between 0 and 4 (Fig. 7a–e). However, even if some fraction of Na_2CO_3 remained unreacted during the grinding process in the prepared batches, it would certainly have dissolved during washing after the synthesis due to its high solubility in water. The proposed chemical formula of $NaCO_3$HAp is $Ca_{10-x}Na_{2x/3}(PO_4)_{6-x}(CO_3)_x(H_2O)_x(OH)_{2-x/3}$, where $0 \leqslant x \leqslant 3$, corresponding to the theoretical solubility limit of carbonate in HAp of 22.3 wt% [38].

Thermogravimetric analysis of the as-prepared $NaCO_3$HAp powders (Fig. 8) in the temperature range of 25–950°C confirmed the results of XRD. In all the

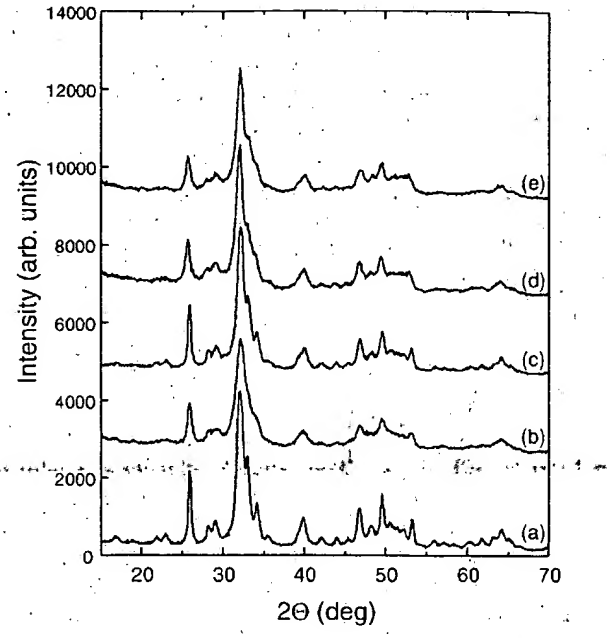

Fig. 7. XRD patterns of the as-prepared $NaCO_3$HAp powders: (a) $x=0$, corresponding to stoichiometric HAp; (b) $x=1$; (c) $x=2$; (d) $x=3$; and (e) $x=4$.

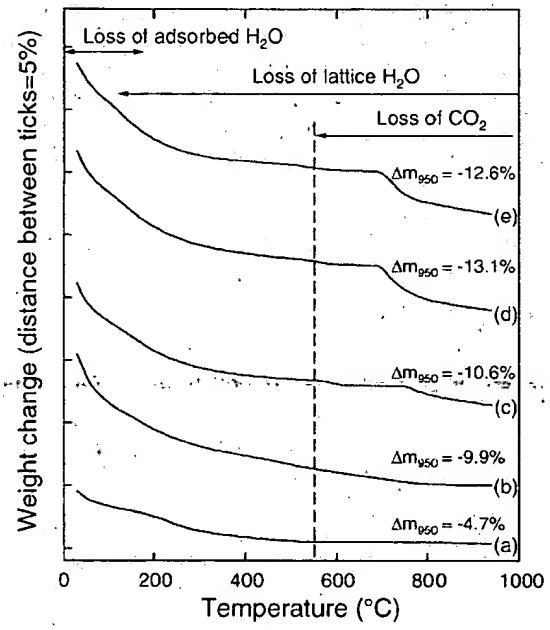

Fig. 8. TG curves of the as-prepared $NaCO_3$HAp powders: (a) $x=0$; (b) $x=1$; (c) $x=2$; (d) $x=3$; and (e) $x=4$. Δm_{950} is a total relative weight change at 950°C. The Δm_{950} values are marked for each powder.

powders, a significant loss of weight was observed up to approximately 450°C and was due to the loss of adsorbed and lattice water [15]. Another weight loss for $NaCO_3$HAp powders occurred above 550°C and was

attributed mainly to the loss of carbonate with subsequent formation of Na_2O and CaO [15]. No weight losses related to the decomposition of Na_2CO_3 (around 400°C), $Ca(OH)_2$ or $CaCO_3$ were observed, which in addition to the XRD data serves as evidence that the as-prepared powders were phase-pure $NaCO_3HAp$.

FTIR results support the TGA and XRD data. The FTIR spectra of the as-prepared $NaCO_3HAp$ powders (Fig. 9) are typical spectra of carbonated HAp showing similar results to those of the CO_3HAp powders. PO_4-derived bands at 478, 566, 605, 963, and 1030–1090 cm^{-1}, CO_3-derived bands at 870 cm^{-1} and around 1420–1480 cm^{-1} [6,15], and adsorbed water bands at 1630 and 3000–3700 cm^{-1} were again observed. Very low intensity of both OH-derived bands at 630 and 3570 cm^{-1}, which are clearly visible only in the nominally stoichiometric HAp powder, and broadening of the PO_4-derived bands with increasing x were observed (Fig. 9). These effects are typical for $NaCO_3HAp$ synthesized by wet methods and can be explained by a decrease in crystallinity due to increased sodium and carbonate substitution in the HAp lattice [6]. Intensity of the adsorbed water bands is much higher in the samples with $x>0$ than in the undoped HAp ($x=0$), therefore very low intensity of the OH-derived bands, particularly in the samples with $x>0$, could be also caused by the presence of large amounts of adsorbed water (Fig. 9, Table 1). The FTIR spectra clearly show that with increasing x in the starting slurry, intensity of the CO_3-derived bands increases which serves as evidence that the amount of carbonate in the HAp lattice increases. Measured concentrations of CO_3 in the $NaCO_3HAp$ powders were between 4.1 wt% for $x=1$ and 12.0 wt% for $x=4$ (Table 1). Thus, the theoretical solubility limit of carbonate in $NaCO_3HAp$ has not been exceeded. Position of the carbonate-derived bands in Fig. 9 indicates dominant CO_3^{2-}-for-PO_4^{3-} substitution with a possibility of partial OH^--for-PO_4^{3-} substitution, as observed also in the CO_3HAp powders.

Heat treatment of the as-prepared $NaCO_3HAp$ powders at 1100°C for 1 h in air resulted in formation of several phases in addition to narrowing their HAp-derived XRD peaks (Fig. 10). At $x=1$, only HAp- and NaOH-derived peaks were observed in the XRD pattern of the heat-treated $NaCO_3HAp$. At $x=2$–4, HAp, NaOH, CaO, and $Ca(OH)_2$ were detected in the heat-treated $NaCO_3HAp$ powders. Intensity of the additional new bands increased with the degree of carbonate substitution (increasing x). The as-prepared $NaCO_3HAp$ powders did not contain any impurity phases, as shown by XRD, TG, and FTIR; therefore, the formation of NaOH, CaO and $Ca(OH)_2$ was a result of decomposition of $NaCO_3HAp$ at high temperature and subsequent storage conditions of the heated powder. The formation of CaO and Na_2O is typically observed upon calcination of $NaCO_3HAp$ [15]. In our experiments, both Na- and Ca-hydroxide phases must have been formed from corresponding oxides during prolonged exposure to moisture from the air upon storage.

Specific surface areas of the as-prepared $NaCO_3HAp$ powders were 91 m^2/g for $x=0$, 117 m^2/g for $x=1$,

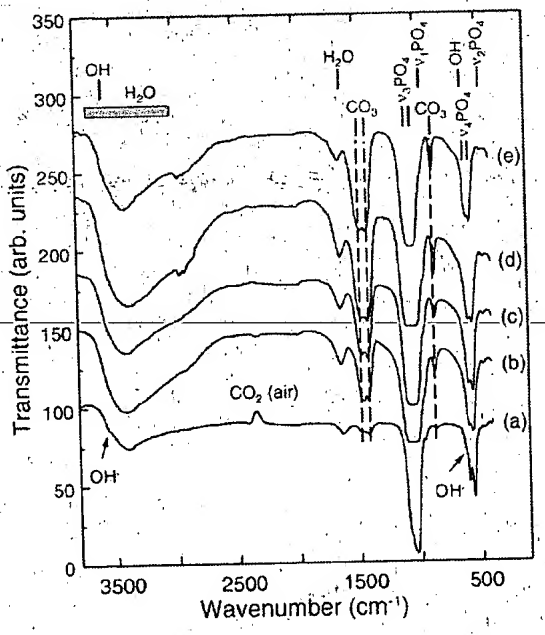

Fig. 9. FTIR spectra of the as-prepared $NaCO_3HAp$ powders: (a) $x=0$; (b) $x=1$; (c) $x=2$; (d) $x=3$; and (e) $x=4$.

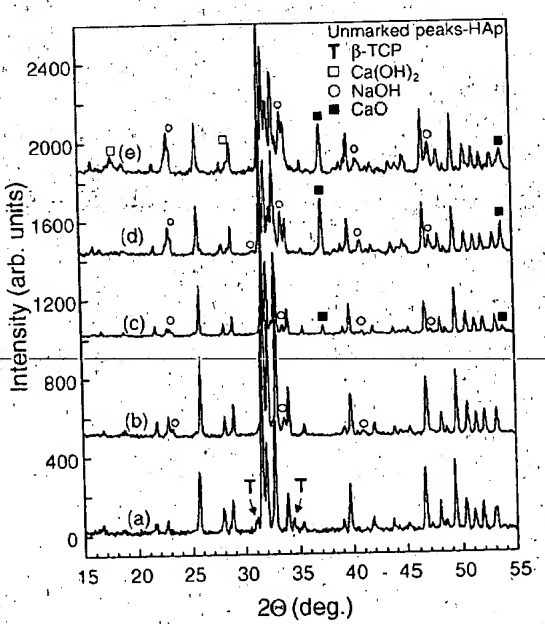

Fig. 10. XRD patterns of the $NaCO_3HAp$ powders after calcination in air at 1100°C for 1 h: (a) $x=0$; (b) $x=1$; (c) $x=2$; (d) $x=3$; and (e) $x=4$.

82 m^2/g for $x=2$, 121 m^2/g for $x=3$, and 86 m^2/g for $x=4$ ($\pm 2\ m^2/g$), which correspond to estimated equivalent spherical diameters (d_{BET}) of 16-23 nm (Table 1). The particle size distributions of the as-prepared $NaCO_3HAp$ powders were in all cases mono-modal with median values of 663 nm for $x=0$, 350 nm for $x=1$, 1625 nm for $x=2$, 1592 nm for $x=3$, and 622 nm for $x=4$ (Table 1). Corresponding average particle sizes were 685 nm for $x=0$, 473 nm for $x=1$, 1285 nm for $x=2$, 1298 nm for $x=3$, and 669 nm for $x=4$ (Table 1). These measurements indicate the presence of aggregates consisting of ≈ 20 nm HAp primary particles. Results of FESEM and TEM observations, shown in Fig. 11, were in good agreement with the results of both BET and DLS measurements. The as-prepared $NaCO_3HAp$ powders contained large aggregates, 1–2 μm in diameter (Fig. 11d), which consisted of nanosized HAp crystals (Fig. 11a–e). The crystal size of the $NaCO_3HAp$ powders that exhibited lower values of the specific surface area, i.e. $x=2$ (Fig. 11b) and $x=4$ (Fig. 11e) appeared larger than the crystals of $NaCO_3HAp$ powders with high specific surface area, i.e. $x=1$ (Fig. 11a) and $x=3$ (Fig. 11c).

3.3. Comparison of CO_3HAp and $NaCO_3HAp$ powders prepared by the mechanochemical–hydrothermal technique

The CO_3HAp and $NaCO_3HAp$ powders synthesized in the present work by the mechanochemical–hydrothermal method share several common features. All of them consist of nanosized crystals forming larger aggregates, which results in broad particle size distributions. In our study, we could not find any correlation between either specific surface area or average grain size and carbonate content (Table 1). Another interesting feature of our powders is that almost all synthesized crystals are equiaxed irrespective of carbonate concentration, including the nominally stoichiometric HAp powder ($x=0$, Fig. 11f). The only exception is the as-prepared CO_3HAp powder prepared at $x=2$, which consisted of elongated aggregates of nanosized needle-like crystals (Fig. 6b). Some of the as-prepared CO_3HAp and $NaCO_3HAp$ powders, however, contained a significant fraction of elongated aggregates of equiaxed crystals, as shown in Figs. 6a and 11b. Our results are generally in contradiction to other studies, which report decrease of the crystal aspect ratio with increasing carbonate concentration in HAp powders prepared by wet methods [6]. Our results have shown that it is possible to prepare nanosized CO_3HAp and $NaCO_3HAp$ crystals with equiaxed morphology and carbonate concentration ranging between 0.8 and 12 wt% by the mechanochemical–hydrothermal method.

The absence of any unreacted species in almost all as-prepared CO_3HAp and $NaCO_3HAp$ powders indicates high efficiency of the mechanochemical–hydrothermal synthesis route at room temperature. Broad XRD peaks can be ascribed to both lattice disorder introduced by the carbonate ions and the very small size of the crystallites. Structural disorder in the as-prepared CO_3HAp and $NaCO_3HAp$ powders has been manifested in the FTIR spectra in the form of broadening of the PO_4-derived bands. Broadening of both XRD peaks and FTIR bands was generally more distinct at higher carbonate concentrations. The XRD and FTIR results in addition to the results of both thermogravimetric analysis and calcination of the synthesized powders at 1100°C for 1 h in air are consistent with the literature data for both CO_3HAp and $NaCO_3HAp$ [15]. Altogether the characterization results of our powders indicate good control and high uniformity of carbonate substitution in all as-prepared powders.

3.4. Mechanism of the mechanochemical–hydrothermal synthesis of HAp and carbonate HAp

Modeling of the mechanochemical–hydrothermal synthesis of CO_3HAp and $NaCO_3HAp$, which was accomplished using OLI Software [39], revealed that in addition to solid carbonated apatites, different species could form as products of the reaction between $Ca(OH)_2/CaCO_3/Na_2CO_3$ and $(NH_4)_2HPO_4$ in water [40]. In the synthesis of CO_3HAp powders, HPO_4^{2-}, NH_4^+, and NH_3 (aq) can form at the concentration level of ≈ 1 m; $NH_2CO_2^+$, HCO_3^-, and CO_3^{2-} can form at the concentration levels of $\approx 10^{-1}$–10^{-2} m. In the synthesis of $NaCO_3HAp$ powders, HPO_4^{2-}, NH_4^+, NH_3 (aq), and Na^+ can form at the concentration level of ≈ 1 m; $NH_2CO_2^+$, HCO_3^-, CO_3^{2-}, $NaCO_3^-$, and $NaHCO_3$ (aq) can form at the concentration levels of $\approx 10^{-1}$–10^{-3} m. Both types of reactions produce also Ca^{2+} and OH^-. Naturally alkaline environments of the syntheses are very important because higher pH values favor formation of the apatite phases [6,15]. The calculations were based upon assumptions that the solid HAp phase had a stoichiometric composition, i.e. $Ca_{10}(PO_4)_6(OH)_2$ and that the reactions occurred under normal conditions (25°C, 1 bar).

The previous mechanochemical and mechanochemical–hydrothermal syntheses of HAp and carbonated HAp powders accomplished using $CaHPO_4 \cdot 2H_2O$ or $Ca(H_2PO_4)_2 \cdot H_2O$ as sources of calcium and phosphorus, $Ca(OH)_2$ and/or $CaCO_3$ as sources of calcium were usually done at room temperature under either dry conditions or in water [18–24]. The as-prepared powders were often nano-sized with considerable aggregation [22, 23]. A common feature of the HAp powders prepared in all the previous works was their very low crystallinity. Another disadvantage of the previously synthesized powders was their high calcium deficiency (Ca/P molar ratio in the range of 1.50–1.64) resulting in partial or

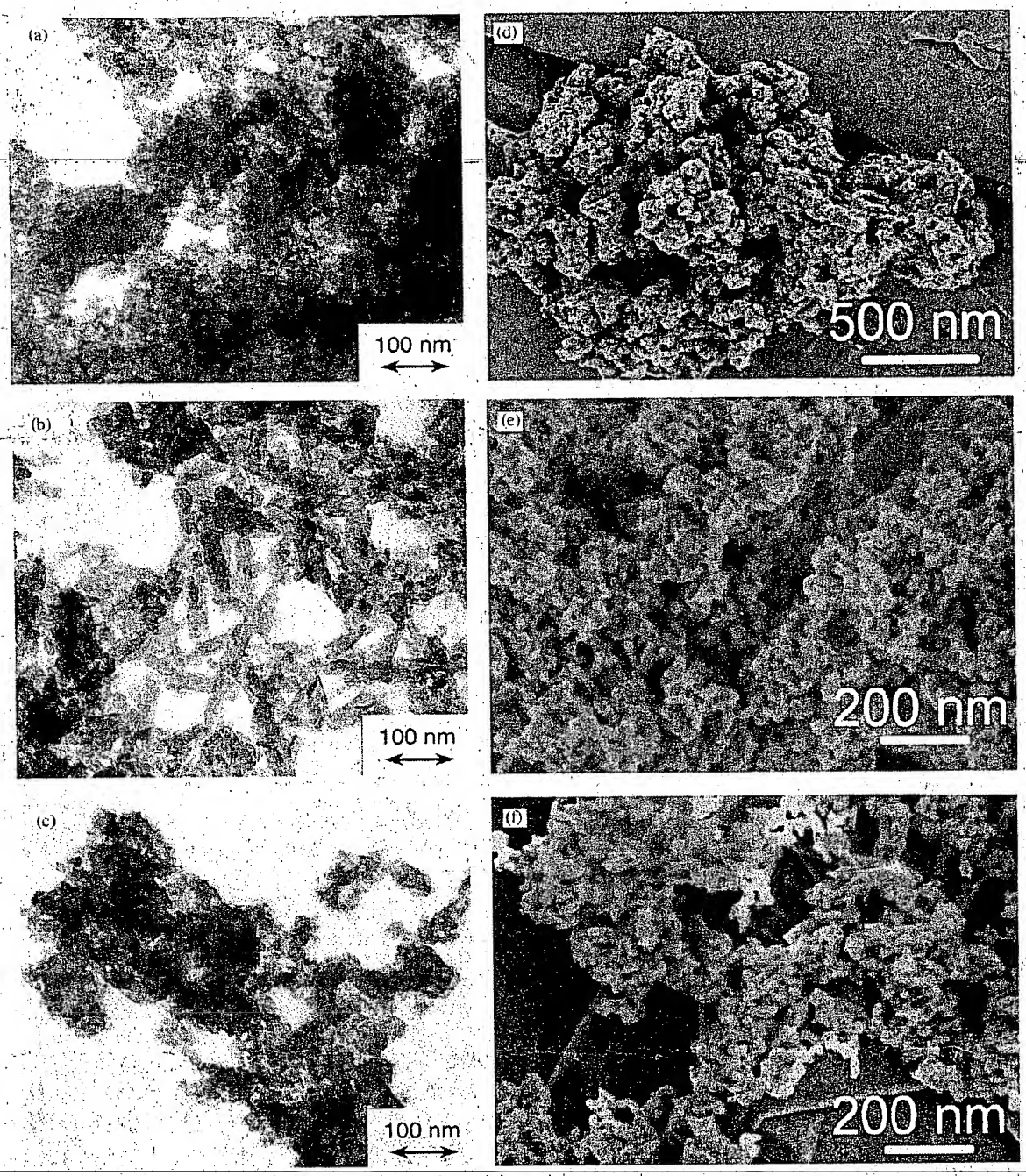

Fig. 11. Electron microscopy photographs of the as-prepared $NaCO_3HAp$ powders showing aggregation of nanosized HAp crystals. TEM: (a) $x=1$, (b) $x=2$, (c) $x=3$. FESEM: (d) $x=4$, (e) $x=4$ and (f) $x=0$.

total transformation into β-TCP ($Ca_3(PO_4)_2$) during calcination at 700–750°C to crystallize all amorphous phases.

Our results emphasize the importance of an aqueous solution, which actively participates in the synthesis reaction by dissolving one of the reactants, which is not observed with conventional mechanochemical synthesis of carbonated HAp. In previous work, the solubilities of mechanochemical reacted powders in 100 ml of water at room temperature are 0.0316, 1.8, 0.185, and 0.0014 g for $CaHPO_4 \cdot 2H_2O$, $Ca(H_2PO_4)_2 \cdot H_2O$, $Ca(OH)_2$, and $CaCO_3$, respectively [41]. In comparison, in this work, the solubilities of $(NH_4)_2HPO_4$ and Na_2CO_3 in water under the same conditions are 57.5 and 30.7 g, respectively [41]. The previous studies on mechanochemical and mechanochemical–hydrothermal synthesis of carbonated HAp did not take advantage of water as a solvent as done in the present work and our earlier

report [25]. While previous mechanochemical–hydrothermal work utilized water as a reaction medium, its effect was limited by much lower solubility of the starting powders (between 0.0014 and 1.8 g in 100 ml of water at room temperature). This may be the reason why the carbonated HAp powders previously synthesized by both methods [18–24] were highly calcium deficient and had very low crystallinity.

4. Summary

Our work demonstrates the applicability of mechanochemical–hydrothermal synthesis for preparations of carbonated HAp powders. Crystalline CO_3HAp and $NaCO_3$HAp powders with carbonate concentration ranging between 0.8 and 12 wt% have been prepared by the mechanochemical–hydrothermal route at room temperature. The powders consisted of equiaxed crystals, ≈20 nm in diameter, which formed larger aggregates resulting in median particle size in the range of 350 nm–1.63 μm. This process is advantageous over previous work since water actively participates in the synthesis by both dissolving some of the reacting powders and serving as a reaction medium.

Acknowledgements

This research was supported by the Johnson & Johnson Corporate Biomaterials Center and the Center for Biomedical Devices at Rutgers University. The authors are greatly indebted to James Kim for experimental assistance, Chun-Wei Chen for obtaining TEM images, Eric Gulliver for FESEM images, and Charles Oakes for thermodynamic calculations.

References

[1] Aoki H. Science and medical applications of hydroxyapatite. Tokyo, Japan: Japanese Association of Apatite Science, 1991.
[2] Hench LL. Bioceramics: from concept to clinic. J Am Ceram Soc 1991;74:1487–510.
[3] Suchanek W, Yoshimura M. Processing and properties of hydroxyapatite-based biomaterials for use as hard tissue replacement implants. J Mater Res 1998;13:94–117.
[4] TenHuisen KS, Martin RI, Klimkiewicz M, Brown PW. Formation and properties of a synthetic bone composite: hydroxyapatite-collagen. J Biomed Mater Res 1995;29:803–10.
[5] Doi Y, Shibutani T, Moriwaki Y, Kajimoto T, Iwayama Y. Sintered carbonate apatites as bioresorbable bone substitutes. J Biomed Mater Res 1998;39:603–10.
[6] LeGeros RZ. Calcium phosphates in oral biology and medicine. Basel, Switzerland: Karger AG, 1991.
[7] Doi Y, Iwanaga H, Shibutani T, Moriwaki Y, Iwayama Y. Osteoclastic responses to various calcium phosphates in cell cultures. J Biomed Mater Res 1999;47:424–33.
[8] Redey SA, Nardin M, Bernache-Assolant D, Rey C, Delannoy P, Sedel L, Marie PJ. Behavior of human osteoblastic cells on stoichiometric hydroxyapatite and type A carbonate apatite: role of surface energy. J Biomed Mater Res 2000;50:353–64.
[9] Barralet J, Akao M, Aoki H, Aoki H. Dissolution of dense carbonate apatite subcutaneously implanted in Wistar rats. J Biomed Mater Res 2000;49:176–82.
[10] Ellies LG, Carter JM, Natiella JR, Featherstone JDB. Quantitative analysis of early in vivo tissue response to synthetic apatite implants. J Biomed Mater Res 1988;22:137–48.
[11] SRS® Skeletal Repair System® Cement, Norian Corporation, CA, USA. PMA Number P970010. Approved by Food and Drug Administration (FDA) on 23 December 1998.
[12] Schildhauer TA, Bennett AP, Wright TM, Lane JM, O'Leary PF. Intravertebral body reconstruction with an injectable in situ-setting carbonated apatite: biomechanical evaluation of a minimally invasive technique. J Orthop Res 1999;17:67–72.
[13] Lotz JC, Hu SS, Chiu DF, Yu M, Colliou O, Poser RD. Carbonated apatite cement augmentation of pedicle screw fixation in the lumbar spine. Spine 1997;22:2716–23.
[14] Du C, Cui FZ, Feng QL, Zhu XD, de Groot K. Tissue response to nano-hydroxyapatite/collagen composite implants in marrow cavity. J Biomed Mater Res 1998;42:540–58.
[15] Elliott JC. Structure and chemistry of the apatites and other calcium orthophosphates. Amsterdam: Elsevier, 1994.
[16] Suchanek W, Suda H, Yashima M, Kakihana M, Yoshimura M. Biocompatible whiskers with controlled morphology and stoichiometry. J Mater Res 1995;10:521–9.
[17] Jaffe EB. Abstracts of the literature on synthesis of apatites and some related phosphates. Geological Survey Circular 1951;135.
[18] Toriyama M, Kawamura S. Synthesis of β-tricalcium phosphate by use of wet milling. J Ceram Soc Jpn 1986;94:1004–7.
[19] Toriyama M, Kawamura S. Sinterable powder of mechanochemically synthetic β-tricalcium phosphate. J Ceram Soc Jpn 1987;95:741–5.
[20] Toriyama M, Kawamura S, Ito Y, Nagae H. Thermal change of calcium deficient apatite obtained by mechanochemical treatment. J Ceram Soc Jpn 1989;97:554–8.
[21] Otsuka M, Matsuda Y, Hsu J, Fox JL, Higuchi WI. Mechanochemical synthesis of bioactive material: effect of environmental conditions on the phase transformation of calcium phosphates during grinding. Biomed Mater Eng 1994;4:357–62.
[22] Toriyama M, Ravaglioli A, Krajewski A, Galassi C, Roncari E, Piancastelli A. Slip casting of mechanochemically synthesized hydroxyapatite. J Mater Sci 1995;30:3216–21.
[23] Toriyama M, Ravaglioli A, Krajewski A, Celotti G, Piancastelli A. Synthesis of hydroxyapatite-based powders by mechanochemical method and their sintering. J Eur Ceram Soc 1996;16:429–36.
[24] Yokogawa Y, Toriyama M, Kawamoto Y, Suzuki T, Nishizawa K, Nagata F, Mucalo MR. Preparation of calcium strontium apatite through mechanochemical method. Chem Lett 1996; 1:91–2.
[25] Shuk P, Suchanek WL, Hao T, Gulliver E, Riman RE, Senna M, TenHuisen KS, Janas VF. Mechanochemical–hydrothermal preparation of crystalline hydroxyapatite powder at room temperature. J Mater Res 2001;16:1231–4.
[26] Gutman E. Mechanochemistry of materials. Cambridge, UK: Cambridge International Science Publishing, 1997.
[27] Watanabe T, Isobe T, Senna M. Mechanisms of incipient chemical reaction between $Ca(OH)_2$ and SiO_2 under moderate mechanical stressing: II. Examination of a radical mechanism by an EPR study. J Solid State Chem 1996;122:291–6.
[28] Komatsubara S, Isobe T, Senna M. Effect of preliminary mechanical treatment on the microhomogenization during

heating of hydrous gels as precursors for lead titanate. J Am Ceram Soc 1994;77:278–82.
[29] Baek JG, Isobe T, Senna M. Synthesis of pyrochlore-free $0.9Pb(Mg_{1/3}Nb_{2/3})O_3$-$0.1PbTiO_3$ ceramics via a soft mechanochemical route. J Am Ceram Soc 1997;80:973–81.
[30] Yoshimura M, Suchanek W. In situ fabrication of morphology-controlled advanced ceramic materials by soft, solution processing. Solid State Ion 1997;98:197–208.
[31] Kosova NV, Khabibullin AKh, Boldyrev VV. Hydrothermal reactions under mechanochemical treating. Solid State Ion 1997;101–103:53–8.
[32] Byrappa K, Yoshimura M. Handbook of hydrothermal technology. New Jersey: William Andrews Publishing, LLC/Noyes Publications, 2001.
[33] Hamada K, Senna M. Mechanochemical effects on the properties of starting mixtures for $PbTiO_3$ ceramics by using a novel grinding equipment. J Mater Sci 1996;31:1725–8.
[34] Huffman Jr. EWD. Performance of a new automatic carbon dioxide coulometer. Microchem J 1977; 22: 567-573.
[35] Kühl G von, Nebergall WH. Hydrogenphosphat- und Carbonapatite. Z Anorg Allg Chem 1963;324:313–20.
[36] Royer A, Viguie JC, Heughebaert M, Heughebaert JC. Stoichiometry of hydroxyapatite: influence of the flexural strength. J Mater Sci Mater Med 1993;4:76–82.
[37] Ślósarczyk A, Stobierska E, Paszkiewicz Z, Gawlicki M. Calcium phosphate materials prepared from precipitates with various calcium: phosphorus molar ratios. J Am Ceram Soc 1996;79:2539–44.
[38] Bonel G, Labarthe JC, Vignoles C. Contribution à l'étude structurale des apatites carbonaté es de type B. Physico-Chimie et Cristallographie des Apatites d'Intérêt Biologique, Colloques Internationaux du Centre National de la Recherche Scientifique No. 230 Paris, 1973. Paris, CNRS, 1975, p. 117–125.
[39] Environmental and Corrosion Simulation programs (ESP/CSP), OLI Systems, Inc., Morris Plains, NJ, 1996.
[40] Oakes C, Private Communication, 2000.
[41] Weast RC, Astle MJ, Beyer WH, editors. CRC handbook of chemistry and physics, 68th Edition (1987–1988). Boca Raton, FL: CRC Press, 1987.